Integrated bi-directional vibration control and energy harvesting of monopile offshore wind turbines

Article *in* Ocean Engineering · March 2019

DOI: 10.1016/j.oceaneng.2019.02.015

2 authors:

Vahid Jahangiri
Louisiana State University
10 PUBLICATIONS **64** CITATIONS
SEE PROFILE

Chao Sun
Louisiana State University
27 PUBLICATIONS **268** CITATIONS
SEE PROFILE

Integrated Bi-Directional Vibration Control and Energy Harvesting of Monopile Offshore Wind Turbines

V. Jahangiri[a], C. Sun[a,*]

[a]*Department of Civil and Environmental Engineering, Louisiana State University, Baton Rouge, Louisiana 70803, USA*

Abstract

Offshore wind turbines (OWTs) subjected to combined wind and wave loadings experience excessive bi-directional vibrations that adversely influence the system performance and the structural integrity. The present paper utilizes a three-dimensional pendulum tuned mass damper (3d-PTMD) to mitigate the bidirectional vibrations as well as harvest the kinetic energy using a linear electromagnetic energy harvester. The proposed energy harvester consists of magnets and coil assemblies which are connected with the pendulum to convert the kinetic energy of the pendulum into electricity. An analytical model of the offshore wind turbine coupled with the 3d-PTMD is established using Euler-Lagrangian equation. The mathematical model of the linear electromagnetic energy harvester is established and integrated with the wind turbine model. The optimum design of the electromagnetic energy harvester to minimize the nacelle displacement RMS as well as to maximize the energy output is determined via a numerical search method. The NREL 5 MW baseline wind turbine model is utilized to evaluate the performance of the 3d-PTMD and the energy harvester. Results show that the 3d-PTMD can reduce the bi-directional vibrations induced by misaligned wind and wave loadings. Additionally, electrical energy in orders of magnitude of kilowatts can be harnessed via using the energy harvester.

Keywords: Offshore wind turbines; three-dimensional pendulum tuned mass damper; energy harvesting; bi-directional vibration mitigation; electromagnetic generator

1. Introduction

Increasing demand for renewable energy makes wind energy production grow exponentially in the world today. Offshore wind turbines (OWTs) are becoming increasingly attractive than their onshore counterparts due to steadier and higher wind speeds, fewer space limitations, lower visual impact and less noise pollution in the marine area. However, because of the severe marine conditions such as strong wind, wave and storm surge, the OWTs always suffer from excessive vibrations which will compromise the power output, reducing the structure reliability and increasing the maintenance cost. In this regard, structural control and health monitoring of OWTs have been studied actively by researchers in the past years. In the community of structural control, dissipating the kinetic energy of the main structure by means of viscous dampers is widely used to mitigate the structural response. Alternatively, the kinetic energy of the main structure (especially large structures) can be harnessed as renewable energy. Meanwhile, application of SHM to the OWTs is essential to ensure the wind turbine performance and structural integrity, which requires a large number of sensors. Continuous and reliable power supply to these sensors is a challenge due to limited lifespan of batteries and several miles distance from the coast. Therefore, an integration vibration control and energy harvesting is investigated to reduce the structural response of OWTs and simultaneously supply energy for SHM system.

*Corresponding author
Email address: csun@lsu.edu (C. Sun)

To mitigate the excessive vibration of OWTs, structural vibration control which has been previously applied in traditional civil structures is being studied. Numerous controlling methods have been investigated for offshore wind turbines. Murtagh *et al.* [1] studied the control of the wind turbine along wind vibration using a passive tuned mass damper. Colwell and Basu [2] studied the vibration reduction of the offshore wind turbines using the tuned liquid column damper. It was found that the tuned liquid column damper can increase the tower fatigue life. Although passive control strategies are effective within the targeted frequency range, they might lose part of their effectiveness because of environmental and system variations. To overcome this issue, Lackner and Rotea [3] investigated active control for a floating barge-type wind turbine. It was found that active control is more effective than passive control in mitigating the structural vibrations. Staino *et al.* [4] used active tendons installed inside the wind turbine blades to mitigate the blades edgewise vibration. It was shown that the introduced active control improves the wind turbine blades response. Fitzgerald *et al.* [5] used an active tuned mass damper to mitigate the blades in-plane vibrations. It was concluded that active tuned mass damper is more effective than passive tuned mass damper.

In addition to active control, semi-active control which can provide comparable mitigation effect yet requires orders of magnitude smaller input energy is studied to mitigate the OWTs vibrations considering environmental and system variations. Sun [6, 7] introduced a semi-active TMD (STMD) with tunable damping ratio and natural frequency to mitigate the OWT vibrations. The author found that with damage presence, the passive TMD becomes off-tuned and loses part of its effectiveness. In comparison, the STMD can effectively mitigate the structural vibration in the presence of damage. Dinh *et al.* [8] used an STMD placed in the wind turbine blades, nacelle and platform. It was observed that the semi-active tuned mass damper is more effective than the passive TMD when subjected to time-variant mooring cable tension, rotor speed and blade stiffness.

While most of the current research focuses on mitigating the vibration in the fore-aft direction, OWTs always suffer from significant side-side vibrations due to vortex induced vibrations or misalignment between wind and wave. To address this issue, Lackner and Rotea [9] used dual linear TMDs to control the bi-directional structural vibrations. It was concluded that the dual linear TMDs can improve the structural response in both directions. However, several limitations such as high cost of installation, larger mass and space exist in their approach. Hence, using a tuned mass damper which is capable of mitigating the bi directional vibrations simultaneously is desired. In this regard, Sun and Jahangiri [10, 11] introduced a three dimensional pendulum tuned mass damper (3d-PTMD) to control the excessive vibrations of the monopile OWT in two directions. The two linear TMDs introduced in Ref. [9] was also used for comparison.The authors concluded that the proposed 3d-PTMD is more effective than the dual linear TMDs in mitigating the bi-directional structural vibration.

In the aforementioned literatures, viscous dampers are employed with TMDs to dissipate the kinetic energy into heat by inelastic deformation [12]. Instead of dissipating the kinetic energy into heat, the kinetic energy can be harnessed by means of energy harvesters, i.e. electromagnetic generators, which function as equivalent as viscous dampers from the structural control perspective.

Xie *et al.* [13] introduced a new method by implementing piezoelectric materials to convert the kinetic energy of a high-rise building into electrical power. It was concluded that the introduced method is capable of mitigating the vibration of the building like a TMD. Shen *et al.* [14] proposed a self-powered planar pendulum TMD vibration control and monitoring system. It was found that the proposed system provides a solution to the power supply problem and stimulates the integrated vibration control and monitoring system. Tang and Zuo [15] presented a method to scavenge the vibration energy from tall buildings with TMDs by replacing the traditional viscous dampers with linear electromagnetic devices. The approach was tested in a prototype building and an amount of 60mW energy was harvested from the prototype model. Arias *et al.* [16] studied the feasibility of using passive electromagnetic damping system as a structural device in a traditional civil structure. The authors found that the electromagnetic damping system could operate as a semi-active damper by modifying the circuit impedance. Jahangiri *et al.* [17] employed piezoelectric materials in offshore oil platforms to convert mechanical energy of sea waves into electrical energy. Also, fault diagnosis of the oil platform was studied based on the voltage signal in the presence of different uncertainties. Muliawan *et al.* [18] considered a combination of a spar type floating wind turbine and a floating point absorber wave energy

converter. It was shown that the combination of wave energy converter with the floating wind turbine can increase the total energy production.

A literature review in this area shows that harvesting energy from the motion of a three dimensional pendulum applied in OWTs has not been investigated before. The present paper employs a three-dimensional PTMD (3d-PTMD) proposed in [10] to achieve integrated bi-directional vibration mitigation and energy harvesting of the monopile OWT. On the basis of the authors' previous work [10, 19, 20], first, a nonlinear mathematical model of the monopile OWT coupled with the 3d-PTMD and an energy harvester is established. Next, dynamic interaction between the blades and the tower and the 3d-PTMD is modeled. Then, the mathematical model of a linear electromagnetic energy harvester system consisting of magnets and coil assemblies coupled with the 3d-PTMD is established. The generated electrical power is determined. Finally, the performance of the 3d-PTMD with an energy harvester in mitigating the vibrations in fore-aft and side-side directions is evaluated and compared with an uncontrolled OWT. Results show that the 3d-PTMD with an energy harvester is capable of mitigating the bi-directional vibrations of the OWT in the under misaligned wind and wave loadings. More importantly, electrical power in orders of magnitude of kilowatts can be harvested through the linear electromagnetic energy harvester, which can be used to power the sensors for online structural health monitoring and the actuators for structural control.

2. Establishment of the Analytical Model

Euler-Lagrangian equation is used to establish the equations of motion of a fully coupled three dimensional dynamic model for a monopile OWT with and without the 3d-PTMD. Fig. 1 portrays the schematic model of the OWT with a 3d-PTMD placed in the nacelle. Totally, the coupled system contains 14 degree of freedom (DOF) with $q_1 \sim q_6$ representing the blade in-plane and out-of-plane coordinate, $q_9 \sim q_{12}$ representing the nacelle fore-aft and side-side coordinate, representing the translational and rotational coordinates of the foundation and q_{13} and q_{14} representing the relative coordinate of the PTMD with respect to the nacelle. The soil effects in this paper is modeled with a pair of springs and dash-pots. The stiffness coefficient of soil effects for translational coordinates is represented by k_x and k_y and rotational springs with coefficients of $k_{x\phi}$ and $k_{y\phi}$. Similarly, the damping coefficients for translational coordinates is represented by c_x and c_y and rotational springs with coefficients of $c_{x\phi}$ and $c_{y\phi}$.

In Fig. 1(a), wind-wave misalignment is considered and denoted as β . As shown in Fig. 1(b), a local coordinate system $x_r y_r z_r - o_r$ originating at the rest position of the pendulum is defined where the 3d-PTMD will move along a spherical surface when the nacelle moves in the fore-aft and side-side directions. As illustrated in Fig. 1(c) and (d), two electromagnetic energy harvesters which performs as equivalent as viscous dampers, are attached to the pendulum with an equivalent damping coefficients of $c_{eh,x}$ and $c_{eh,y}$, in x_r and y_r directions respectively. The equations and schematic model of the electromagnetic energy harvester will be presented in section 4.

2.1. Model Description

The Euler-Lagrangian equation is used to establish the equations of motion of the monopile OWT coupled with 3d-PTMD.

$$\frac{d}{dt}\frac{\partial T(t,\tilde{q}(t),\dot{\tilde{q}}(t))}{\partial \dot{q}_i(t)} - \frac{\partial T(t,\tilde{q}(t),\dot{\tilde{q}}(t))}{\partial q_i(t)} + \frac{\partial V(t,\tilde{q}(t))}{\partial q_i(t)} = Q_i(t) \tag{1}$$

where Sign $\dot{()}$ denotes the first derivative with respect to time. T and V are the kinetic and potential energy of the wind turbine, $\tilde{q}(t)$ is the generalized coordinates vector, $Q_i(t)$ is the generalized force corresponding to the i^{th} component of $\tilde{q}(t)$.

The nacelle absolute displacement in fore-aft u_{nac}^{fa} and side-side u_{nac}^{ss} directions can be determined as:

$$\begin{aligned} u_{nac}^{fa} &= q_7 + q_9 + h\tan(q_{10}) \approx q_7 + q_9 + hq_{10} \\ u_{nac}^{ss} &= q_8 + q_{11} + h\tan(q_{12}) \approx q_8 + q_{11} + hq_{12} \end{aligned} \tag{2}$$

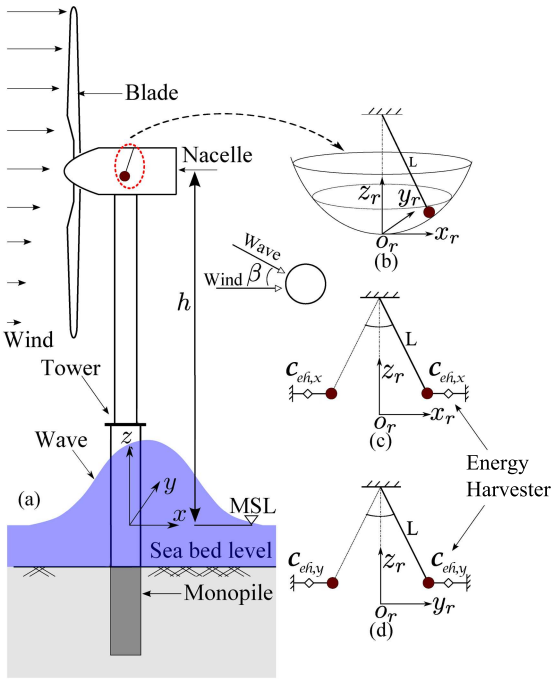

Figure 1: (a): Schematic model of the monopile OWT coupled with the 3d-PTMD; (b): configuration of the pendulum damper; (c): pendulum-energy harvester model in xz plane; (d): pendulum-energy harvester model in yz plane.

By taking the derivative of Eq. (2), the absolute velocity in both directions can be found and the resultant nacelle absolute velocity, v_{nac} , can be determined as:

$$\begin{aligned} v_{nac}^{fa} &= \dot{q}_7 + \dot{q}_9 + h\dot{q}_{10} \\ v_{nac}^{ss} &= \dot{q}_8 + \dot{q}_{11} + h\dot{q}_{12} \end{aligned} \tag{3}$$

By considering parameter Ω as the rotating speed of the blades, the azimuth angle $\psi_j(t)$ of the j^{th} blade can be expressed as:

$$\psi_j = \Omega t + \frac{2\pi}{3}(j-1),\ j = 1, 2, 3 \tag{4}$$

The absolute coordinate of the PTMD can be expressed as:

$$\begin{aligned} x_p &= u_{nac}^{fa} + x_r \\ y_p &= u_{nac}^{ss} + y_r \\ z_p &= L - \sqrt{L^2 - x_r^2 - y_r^2} \end{aligned} \tag{5}$$

The kinetic energy of the pendulum is determined as follows:

$$\begin{aligned} T_p &= \frac{1}{2} m_p (\dot{x}_p^2 + \dot{y}_p^2 + \dot{z}_p^2) \\ &= \frac{m_p}{2} \left[(v_{nac}^{ss})^2 + (v_{nac}^{fa})^2 + 2v_{nac}^{ss}\dot{x}_r + 2v_{nac}^{fa}\dot{y}_r + \dot{x}_r^2 + \dot{y}_r^2 + \frac{(x_r\dot{x}_r + y_r\dot{y}_r)^2}{L^2 - x_r^2 - y_r^2} \right] \end{aligned} \tag{6}$$

where m_p is the mass of the 3d-PTMD.

Finally, the kinetic energy of the wind turbine system with coupled 3d-PTMD can be determined as

follows:

$$T = \frac{1}{2}\sum_{j=1}^{3}\int_0^R \bar{m}v_{bj}^2(r,t)dr + \frac{1}{2}M_{nac}v_{nac}^2 + \frac{1}{2}\int_0^h \bar{M}v_{tow}^2 dz + \frac{1}{2}M_f[\dot{q}_9^2(t)+\dot{q}_{11}^2(t)] + \frac{1}{2}I_f[\dot{q}_{10}^2(t)+\dot{q}_{12}^2(t)] + T_p \quad (7)$$

where M_f and I_f are the foundation mass and moment of inertia respectively; M_{nac} is the nacelle mass; $\bar{m}$ and $\bar{M}$ are the mass density per length of the blade and the tower. Parameters v_{bj} and v_{tow} are the absolute velocity of the blade and tower respectively which can be found in Ref. [6].

Also, the potential energy of the pendulum is expressed as follows:

$$V_p = m_p g(L - \sqrt{L^2 - x_r^2 - y_r^2}) \quad (8)$$

Therefore, the total potential energy of the system can be expressed as:

$$V = V_b + \frac{1}{2}k_t^{fa}q_7^2(t) + \frac{1}{2}k_t^{ss}q_8^2(t) + \frac{1}{2}k_x q_9^2(t) + \frac{1}{2}k_y q_{11}^2(t) + \frac{1}{2}k_{x\phi}q_{10}^2(t) + \frac{1}{2}k_{y\phi}q_{12}^2(t) + V_p \quad (9)$$

where V_b is the potential energy of the blades which can be found in Ref. [6],k_t^{fa} and k_t^{ss} are the fore-aft and side-side stiffness of the tower.

By substituting Eqs. (7) and (9) into Eq. (1), the equations of motion for the OWT can be expressed in a matrix format as follows:

$$\tilde{M}\ddot{\tilde{q}} + \tilde{C_{eq}}\dot{\tilde{q}} + \tilde{K}\tilde{q} = \tilde{Q}_{wind} + \tilde{Q}_{wv} + \tilde{F} \quad (10)$$

where the system mass, damping and stiffness matrices are shown with $\tilde{M}$,$\tilde{C_{eq}}$ and $\tilde{K}$ respectively. In $\tilde{C_{eq}}$, the damping coefficient of the pendulum is determined via the electromagnetic force. $\tilde{F}$ is the generalized force caused by the nonlinearity of the pendulum. Variables $\tilde{Q}_{wind}$ and $\tilde{Q}_{wv}$ are the wind and wave generalized force vectors, which are explained in the next section. It should be noted that Eq.(10) is nonlinear equation since $\tilde{M}$, $\tilde{C_{eq}}$ and $\tilde{K}$ are time-variant.

3. Loading

The wind and wave loadings are derived and presented in this section.

3.1. Wind and Aerodynamic Loading

The derivation of the generalized force vector of the wind loading represented by $\tilde{Q}_{wind}$ in Eq.(10) is presented in this section. A three-dimensional wind field model is used to generate the wind speed time history for each blade element.

The wind velocity $v(z,t)$ can be expressed as: $\tilde{v}(z,t)$, i.e.

$$v(z,t) = \bar{v}(z) + \tilde{v}(z,t) \quad (11)$$

where $\bar{v}(z)$ is the constant mean velocity which is calculated using the logarithmic wind profile. The turbulent component is shown with $\tilde{v}(z,t)$.

For the wind turbulence model and detailed description with respect to the generation of a three dimensional wind field, one can refer to Ref. [10]. Based on Ref. [10], a three dimensional wind field profile represented by 31×31 velocity grids covering the domain of the rotor disk is generated using the TurbSim program [21] as shown in Fig. 2 where the wind velocity is mapped onto the rotating blades. Wind shear power law with an exponent of 0.1 is used to describe the mean wind velocity. The generated full wind field profile is mapped to each span station of the rotating blades using developed MATLAB codes. Fig. 3 demonstrates the wind velocity time history at the center of the first blade tip element where the mean wind velocity is equal to $\bar{v} = 12m/s$ and the turbulence intensity is equal to $TI = 10\%$.

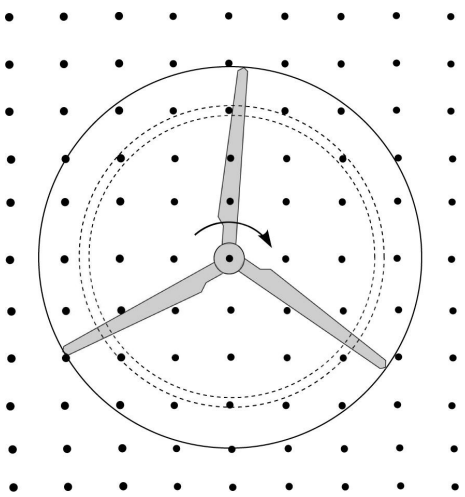

Figure 2: Three dimensional wind profile and the rotating blades.

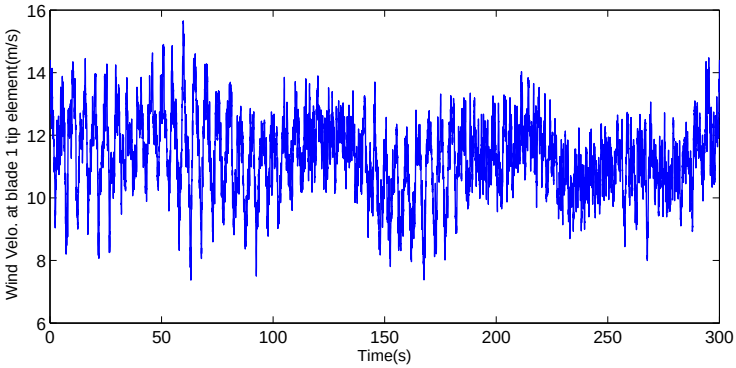

Figure 3: Wind velocity time history at the tip element of first blade($\bar{v} = 12m/s$ at hub height and $TI = 10\%$).

In this study, the Blade Element Momentum (BEM) method is implemented to calculate the aerodynamic loading applied to the rotating blades. The blade rotational, wind speed and the geometry of the blade are considered as input parameters [22].

A general turbine blade is illustrated in Fig. 4. The blade is discretized into N elements and the blade elements are analyzed using BEM method. Parameter R and Ω are the rotor radius and rotation velocity respectively. Also, the i^{th} blade element at a distance r is detailed where dr is the element span and chord length at the element mid-span is shown with $c(r)$.

Fig. 5 demonstrates an arbitrary wind turbine blade element subjected to aerodynamic loading and local velocities. The relative wind velocity can be expressed as:

$$V_{rel} = \sqrt{[v(1-a)]^2 + [\Omega r(1+a')]^2} \tag{12}$$

where a and a' denote the axial velocity and tangential velocity induction factors.

The flow angle ϕ is obtained as:

$$\phi = tan^{-1}\frac{v(1-a)}{\Omega r(1+a')} \tag{13}$$

The attack angle α between the chord line and the relative velocity can be calculated by:

$$\alpha = \phi - \theta \tag{14}$$

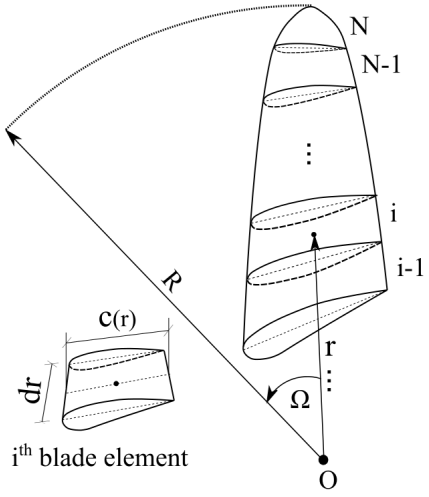

Figure 4: Wind turbine blade discretized into N blade elements.

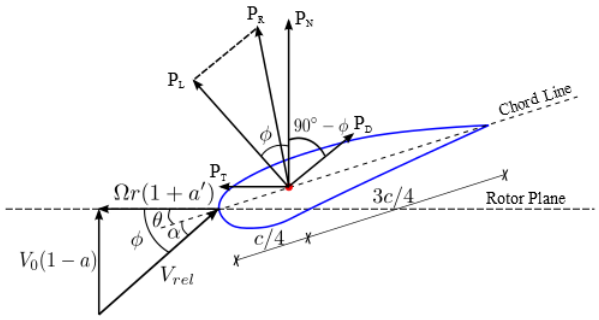

Figure 5: A section of wind turbine blade element subjected to aerodynamic loading and local velocity.

where θ can be calculated by summing the twist and the pitch angle.

The lift and drag coefficients shown with C_l and C_d can be defined from the airfoil data in terms of the attack angle. The lift force P_L and the drag force P_D can be calculated as:

$$P_L = \frac{1}{2}\rho V_{rel}^2 c C_l, \quad P_D = \frac{1}{2}\rho V_{rel}^2 c C_d \tag{15}$$

where ρ and c are the air density and the chord length respectively.

The normal coefficient C_N and the tangential coefficient C_T can be determined as:

$$C_N = cos\phi C_l + sin\phi C_d, \quad C_T = sin\phi C_l - cos\phi C_d \tag{16}$$

The normal force P_N and the tangential forces P_T can be determined as:

$$P_N = \frac{1}{2}\rho V_{rel}^2 c C_N, \quad P_T = \frac{1}{2}\rho V_{rel}^2 c C_T \tag{17}$$

The time series of normal and tangential forces expressed in Eq. (17) can be obtained by developed MATLAB codes based on the introduced algorithm in Ref. [22]. It should be noted that the developed MATLAB code includes Glauert correction and the Prandtl's tip loss factor. In the next step the generalized

aerodynamic loading is calculated based on the Principle of Virtual Work.

The virtual work δW_{wl} done by the wind loading can be defined as:

$$\delta W_{wl} = \sum_{j=1}^{3} \left\{ \int_0^R P_{Tj}(r,t)[\phi_{1e}\delta q_j + \delta u_{nac}^{ss}\cos(\psi_j)]dr + \int_0^R P_{Nj}(r,t)[\phi_{1f}\delta q_{j+3} + \delta u_{nac}^{fa}]dr \right\} \tag{18}$$

where $P_{Tj}(r,t)$ and $P_{Nj}(r,t)$ are the tangential and normal wind loading intensity per unit length on the j^{th} blade.

In terms of the principles of work and energy, the generalized force Q_j can be defined as:

$$Q_j = \frac{\partial(\delta W_{wl})}{\partial(\delta q_j)} \tag{19}$$

The wind induced generalized force can be determined by substituting Eq. (18) into Eq. (19) as follows:

$$\begin{aligned}
Q_{j,wind} &= \int_0^R P_{Tj}(r,t)\phi_{1e}dr,\ Q_{j+3,wind} = \int_0^R P_{Nj}(r,t)\phi_{1f}dr,\ j = 1,2,3 \\
Q_{7,wind} &= \sum_{j=1}^{3}\int_0^R P_{Nj}(r,t)dr,\ Q_{8,wind} = \sum_{j=1}^{3}\int_0^R P_{Tj}(r,t)dr\cos(\psi_j),\ Q_{9,wind} = Q_{7,wind} \\
Q_{10,wind} &= hQ_{7,wind},\ Q_{11,wind} = Q_{8,wind},\ Q_{12,wind} = hQ_{8,wind}
\end{aligned} \tag{20}$$

The magnitude of the wind loading effect on the tower of the offshore wind turbine is relatively small in comparison with the wind turbine blades and thus it is ignored in this paper.

3.2. Wave Loading

The derivation of the generalized force vector of the wave loading represented by $\tilde{Q}_{wave}$ in Eq.(10) is presented in this section. The strip theory and linear wave theory are implemented to determine the wave loading acting on the offshore wind turbine. The monopile fixed offshore wind turbine is a cylindrical structure member. Thus, Morison's equation [23] can be used to estimate the wave loading. The horizontal force of the wave dF acting on a strip of length dz can be expressed as:

$$dF = \frac{\pi D^2}{4}C_M\rho\ddot{u}dz + \frac{\rho}{2}C_D D\dot{u}|\dot{u}|dz \tag{21}$$

where C_M is the mass coefficient which has a value of 1.0 and C_D is the drag coefficient which has a value of 1.2 in this study; ρ is the density of water which is equal to $1025kg/m^3$; D is the diameter of the tower; the wave induced horizontal acceleration and velocity of fluid particles is shown with $\ddot{u}$ and $\dot{u}$.

The JONSWAP wave spectrum Ref. [24] as expressed in the following equation, is used to generate wave time histories.

$$S(f) = 0.3125H_s^2T_p\left(\frac{f}{f_p}\right)^5 exp\left[-\frac{5}{4}\left(\frac{f}{f_p}\right)^{-4}\right](1 - 0.287ln\gamma)\gamma^{exp\left[-\frac{(\omega-\omega_p)^2}{2\sigma^2\omega_p^2}\right]} \tag{22}$$

where H_s denotes the significant wave height, T_p is the period of sea waves, $f_p = 1/T_p$, $\sigma = 0.07$ for $f \le f_p$, $\sigma = 0.09$ for $f > f_p$. Variable γ denotes the JONSWAP peakedness parameter [24]:

$$\gamma = \begin{cases} 5 & T_p/\sqrt{H_s} \le 3.6 \\ exp(5.75 - 1.15T_p/\sqrt{H_s}) & 3.6 < T_p/\sqrt{H_s} \le 5.0 \\ 1 & T_p/\sqrt{H_s} < 5.0 \end{cases} \tag{23}$$

Virtual work δW_{wv} done by the wave loading along the virtual displacement δu_{tow} of the tower can be

expressed as:

$$\delta W_{wv} = \int_0^{\eta} dF \delta u_{tow} = \int_0^{\eta} dF[\phi_{1t}(cos\beta\delta q_7 + sin\beta\delta q_8) + cos\beta(\delta q_9 + z\delta q_{10}) + sin\beta(\delta q_{11} + z\delta q_{12})] \quad (24)$$

The wave generalized force can be determined by substituting Eq. (24) into Eq. (19) as follows:

$$\begin{aligned} Q_{7,wave} &= cos\beta F_{wv,1}, \quad Q_{8,wave} = sin\beta F_{wv,1} \\ Q_{9,wave} &= cos\beta F_{wv,2}, \quad Q_{11,wave} = sin\beta F_{wv,2} \\ Q_{10,wave} &= cos\beta F_{wv,3}, \quad Q_{12,wave} = sin\beta F_{wv,3} \end{aligned} \quad (25)$$

where

$$\begin{aligned} F_{wv,1} &= \int_{-d_w}^{\eta(t)} \phi_{1t}(z) dF = \sum_{i=1}^{N_z} \phi_{1t}(z_i) \left[\frac{\rho\pi D^2(z_i)}{4} C_M \ddot{u}(z_i,t)\Delta z + \frac{\rho}{2} C_D D(z_i)\dot{u}(z_i,t)|\dot{u}(z_i,t)|\Delta z \right] \\ F_{wv,2} &= \int_{-d_w}^{\eta(t)} dF = \sum_{i=1}^{N_z} \left[\frac{\rho\pi D^2(z_i)}{4} C_M \ddot{u}(z_i,t)\Delta z + \frac{\rho}{2} C_D D(z_i)\dot{u}(z_i,t)|\dot{u}(z_i,t)|\Delta z \right] \\ F_{wv,3} &= \int_{-d_w}^{\eta(t)} z dF = \sum_{i=1}^{N_z} \left[\frac{\rho\pi D^2(z_i)}{4} C_M \ddot{u}(z_i,t)\Delta z + \frac{\rho}{2} C_D D(z_i)\dot{u}(z_i,t)|\dot{u}(z_i,t)|\Delta z \right] z_i \end{aligned}$$

Parameter N_z is the number of segments that the wetted portion of the tower is divided and Δz is the segment length.

4. Energy Harvesting

The schematic model of the electromagnetic generator consisting of a magnet assembly and a coil assembly is illustrated in Fig. 6. In the schematic model, the relative motion between the magnet assembly and the coil assembly will produce electrical power. Accordingly, the electromagnetic energy harvester will provide an electromagnetic force to mitigate the motion of the pendulum. One end of the electromagnetic device is hinged to the structure and the other end is hinged to the pendulum. As shown in Fig. 6, the energy harvester can freely rotate along with the motion of the pendulum via using ball hinges.

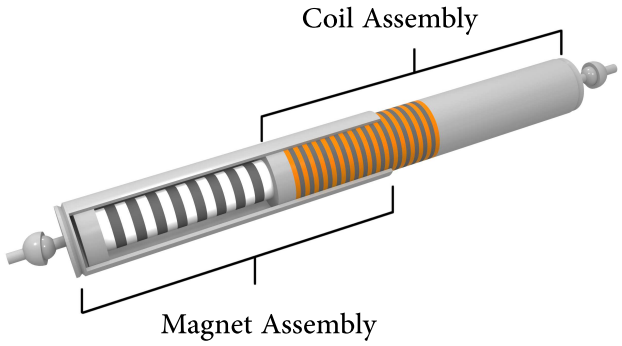

Figure 6: Electromagnetic energy harvester schematic model.

4.1. Uncoupled Equations

Essentially, the dynamic and electrical equations of the energy harvesters are coupled in real time. However, most of existing research simplified the model via considering the two process separately. To reveal the difference and provide more insight into this process, the present paper will establish two models (uncoupled and coupled) and compare the results. In this section, the electromagnetic energy harvester is considered to be uncoupled with the system and the equations are established.

The electrical voltage in x_r and y_r directions produced by the relative motion of the pendulum and the nacelle can be obtained as:

$$\begin{aligned} V_x &= Bl\dot{x}_r \\ V_y &= Bl\dot{y}_r \end{aligned} \tag{26}$$

where parameters B, l, $\dot{x}_r$ and $\dot{y}_r$ are the magnetic field constant, length of the conductor and the relative velocity of the pendulum in x_r and y_r directions.

Using the Ohms law, the electrical current can be determined as:

$$\begin{aligned} I_x &= \frac{V_x}{R_{circuit}} = \frac{B\pi DN\dot{x}_r}{R_{circuit}} \\ I_y &= \frac{V_y}{R_{circuit}} = \frac{B\pi DN\dot{y}_r}{R_{circuit}} \end{aligned} \tag{27}$$

where $R_{circuit}$ is the total resistance and is equal to the sum of internal resistance and the load resistance.

The generated current will cause a magnetic force to oppose the motion of the conductor. According to Lorentz law, the magnetic force is equal to the multiplication of the current, the magnetic field constant and the length of the conductor, which can be expressed as:

$$\begin{aligned} F_x &= \frac{(\pi BDN)^2}{R_{circuit}}\dot{x}_r = c_{eq}\dot{x}_r \\ F_y &= \frac{(\pi BDN)^2}{R_{circuit}}\dot{y}_r = c_{eq}\dot{y}_r \end{aligned} \tag{28}$$

where c_{eq} is an equivalent damping coefficient.

Through solving Eq. (10) numerically, the generated voltage and the corresponding magnetic force can be calculated using Eqs. (26) $\sim$ (28).

4.2. Coupled Equations

In this section, the electromagnetic energy harvester is considered to be coupled with the offshore wind turbine. By coupling the energy harvester with the OWT model, two additional DOFs are added to Eq. (10). The two added DOFs are the current produced by the energy harvester in x_r and y_r directions. An equivalent circuit is shown in Fig. 7 to represent the coupled linear electromagnetic energy harvester which is formulated as follows:

$$\begin{aligned} L_{coil}\dot{I}_x(t) + R_{circ}I_x(t) &= E_x(t) \\ L_{coil}\dot{I}_y(t) + R_{circ}I_y(t) &= E_y(t) \end{aligned} \tag{29}$$

where I_x and I_y are the currents; L_{coil} is the inductance of the coil; E_x and E_y are the electromotive forces in x_r and y_r directions respectively.

The electromagnetic energy harvester is coupled with the OWT system and the electrical current in x_r and y_r directions is considered as two additional DOFs of the system. Hence, the system will have 16 DOFs totally. Parameter L_{coil} is the inductance of the coil and can be determined by the following equation:

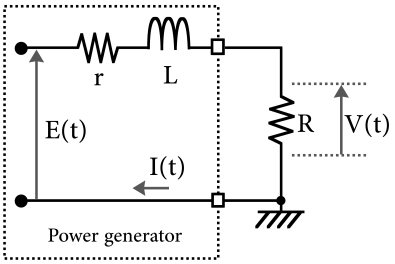

Figure 7: Equivalent electric circuit for power generation.

$$L_{coil} \approx N^2 \mu_0 \mu_r \left(\frac{D}{2}\right)\left(ln\left(\frac{8D}{d}\right) - 2\right) \tag{30}$$

where μ_0 and μ_r are the permeability of free space and relative permeability of the wire.

Based on the Faradays law, the electromotive force is equal to multiplication of electromotive force coefficient (k_{emf}) and the relative velocity:

$$\begin{aligned} E_x(t) &= k_{emf}\dot{x}_r(t) \\ E_y(t) &= k_{emf}\dot{y}_r(t) \end{aligned} \tag{31}$$

The damping force generated by the electromagnetic transducer is expressed as:

$$F_e(t) = k_{emf} I(t) \tag{32}$$

Substituting Eq. (31) into Eq. (29) yields:

$$\begin{aligned} L_{coil}\dot{I}_x(t) + R_{circ} I_x(t) &= k_{emf}\dot{x}_r(t) \\ L_{coil}\dot{I}_y(t) + R_{circ} I_y(t) &= k_{emf}\dot{y}_r(t) \end{aligned} \tag{33}$$

It is noted that the electromagnetic force calculated by Eq. (32) is the equivalent damping force of the pendulum. Then Eqs. (32) and (33) are coupled with Eq. (10) and can be solved numerically simultaneously.

4.3. Energy Harvester Parameters

The optimum design of the electromagnetic energy harvester to minimize the nacelle displacement RMS and to maximize the generated electrical power is presented in this section. A numerical search method is used to determine the optimal parameters for the energy harvester. Variation the energy harvester parameters such as coil diameter, number of turns, circuit resistance and wire diameter is equivalent to change the damping ratio of the 3d-PTMD. On the basis of the authors' previous work [10], a mass ratio of 2% is recommended for the 3d-PTMD considering the mitigation effect and practical constraints. Hence the present study uses a mass ratio of 2%. With the fixed mass ratio of 2%, the optimized frequency ratio was determined to be 0.97. With the given mass ratio (2%) and frequency ratio (0.97), the nacelle displacement RMS and the mean value of generated electrical power corresponding to different damping ratio values are determined. The mean value of generated electrical power and displacement RMS is set as the optimum objective. Fig. 8 demonstrates the nacelle displacement RMS against the damping ratio. From this figure, one can observe that a damping ratio of 10% is the optimum value to minimize the displacement RMS.

Fig. 9 shows the mean value of generated electrical power against the damping ratio. It can be seen that the generated electrical power decreases as the damping ratio decreases. In the present study, the primary objective is to mitigate the wind turbine displacement response. Therefore, optimized value of the damping ratio to minimize the nacelle displacement RMS is selected.

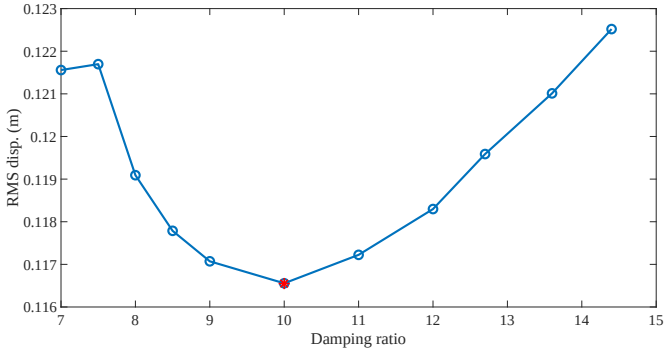

Figure 8: Nacelle displacement RMS with different damping ratio values (The red * denotes the optimum damping ratio that minimizes the response).

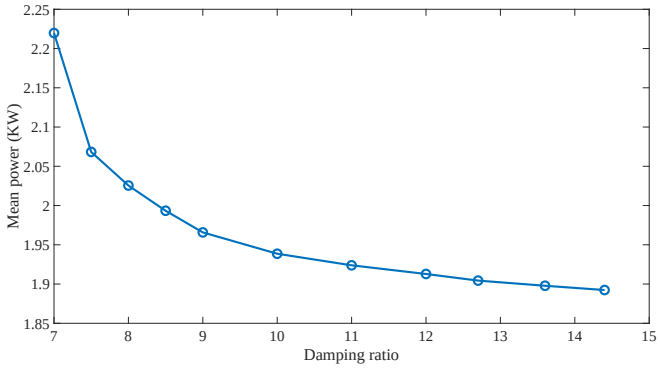

Figure 9: Mean value of generated electrical power with different damping ratio values.

The desired damping ratio for PTMD is set to be 10%. By considering a mass ratio of 2% and $c = 2\xi m_p \omega_n$, the damping coefficient can be calculated as $2852.42 N/sm$. In this regard, the chosen electromagnetic device parameters which satisfy the desired design for damping coefficient are listed in Table. 1.

Table 1: Linear electromagnetic generator design parameters

Parameter name	**Symbol**	**Value**
Coil average diameter	$D\,(mm)$	50
Wire diameter	$d\,(mm)$	1
Number of turns	N	359
Coil resistance	$R_{coil}\,(\Omega)$	1.21
Load resistance	$R_{load}\,(\Omega)$	1.21

5. System Parameters

The parameter values of the baseline monopile OWT, loading parameters and the soil effects are presented in this section. In this paper, the NREL 5MW OC3 monopile wind turbine model [25] is used. The parameters are listed in Table. 2.

The soil effect is modeled with linear springs and dash-pots. To represent the clay soil condition, the spring stiffnesses are equal to, $k_x = k_y = 3.89E9\,N/m$, $k_{x\phi} = k_{y\phi} = 1.14E11\,Nm/rad$. Also, the soil

Table 2: NREL 5-MW baseline wind turbine parameters[25]

Gross properties	Rating	5 MW
	Rotor diameter	$126\,m$
	Hub height	$90\,m$
	Cut-in, rated, cut-out wind speed	$3\,m/s$, $11.4\,m/s$, $25\,m/s$
	Cut-in, rated rotor speed	$6.9\,rpm$, $12.1\,rpm$
Blade	Length	$61.5\,m$
	Mass	$17,740\,kg$
	Second moment of inertia	$11,776\,kgm^2$
Nacelle + hub	Nacelle mass	$240,000\,kg$
	Hub mass	$56,780\,kg$
	Hub diameter	$3\,m$
Tower	Height above ground	$87.6\,m$
	Overall mass	$267,650\,kg$

damping properties are equal to $\zeta_x = \zeta_y = \zeta_{x\phi} = \zeta_{y\phi} = 0.6\%$ [26].

6. Simulation and Results

In this section, the performance of the 3d-PTMD in mitigating the bi-directional vibration of the OWT is evaluated and the harnessed energy from the energy harvester is determined.

Structural responses of the wind turbine are calculated through numerically solving Eq. (10). The mean wind velocity is considered to be $12\,m/s$ with a turbulent intensity of 10% and the significant wave height is assumed to be $2\,m$. Based on preceding discussions, a suggested mass ratio of 2% is utilized and the corresponding optimal frequency ratio and damping ratio are: $f_{opt} = 0.97$ and $\xi_{opt} = 10\%$.

Fig. 10 (a)-(d) shows the nacelle fore-aft displacement time-history comparison between the 3d-PTMD and the uncontrolled OWT under the four wind-wave misalignment angles. It can be found that the 3d-PTMD is able to mitigate the vibrations of the OWT in the fore-aft direction. According to the data presented in Fig. 10, the 3d-PTMD is able to reduce the RMS of nacelle displacement in fore-aft direction by 70%. Fig. 11 (a)-(d) shows the nacelle side-side response mitigation comparison where it is indicated that the 3d-PTMD can mitigate the nacelle side-side response under different wind-wave misalignment angles. The 3d-PTMD is able to mitigate the displacement of OWT in the side-side direction by around 77%. It should be noted that the side-side motion is minimal when the wind and wave loadings are aligned as shown in Fig. 11(a).

Figs. 12 and 13 illustrate the generated voltage time-history comparison between the coupled and uncoupled energy harvester models in the fore-aft and side-side directions under four wind-wave misalignment angles. It should be noted that a 50 s time window is used to show the differences clearly. One can observe the difference between the results from the uncoupled and coupled models. Quantitatively, the generated voltage calculated using the coupled model is 7% smaller than that via the uncoupled model. The reason for the small difference between the coupled and uncoupled energy harvester models is the low frequency feature of the primary structure and the small value of the inductance. The inductance value for the considered electromagnetic damper is equal to 0.02 Hz which is a small value.

The generated power in the fore-aft direction under different wind and wave misalignments is illustrated in Fig. 14 (a)-(d). One can find that the generated electrical power decreases when increasing the wind and wave misalignment angle. The average generated electrical power in fore-aft direction for 0°, 30°, 60° and 90° wind-wave misalignment angle is 792, 594, 203 and 2.8 W respectively.

The generated power in the side-side direction under different wind and wave misalignments is illustrated in Fig. 15 (a)-(d). The average generated electrical power in side-side direction for 0°, 30°, 60° and 90° wind-wave misalignment angle is 0, 205, 615 and 820 W respectively. It can be seen that increasing the wind and wave misalignment angle will result in an increase in the generated electrical power.

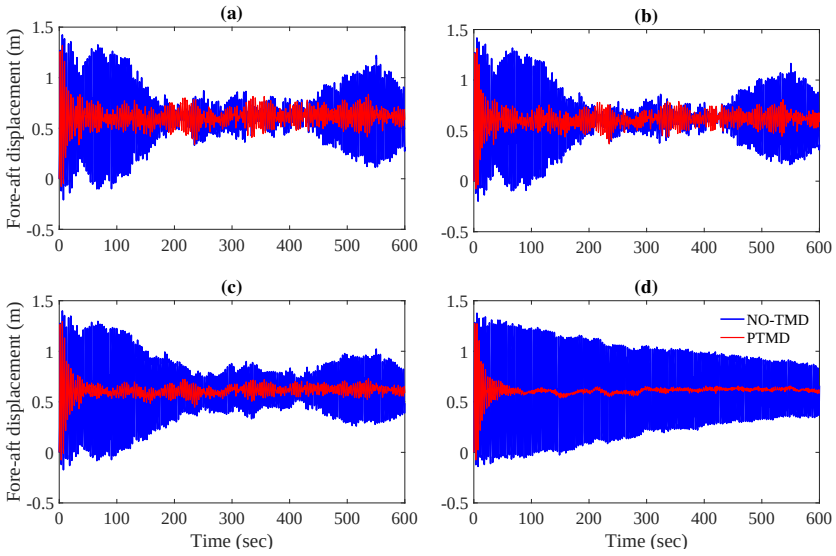

Figure 10: Nacelle fore-aft vibration comparison with and without the 3d-PTMD under four different wind and wave misalignment angles. (a): $\beta = 0°$ (b): $\beta = 30°$, (c): $\beta = 60°$, (d): $\beta = 90°$.

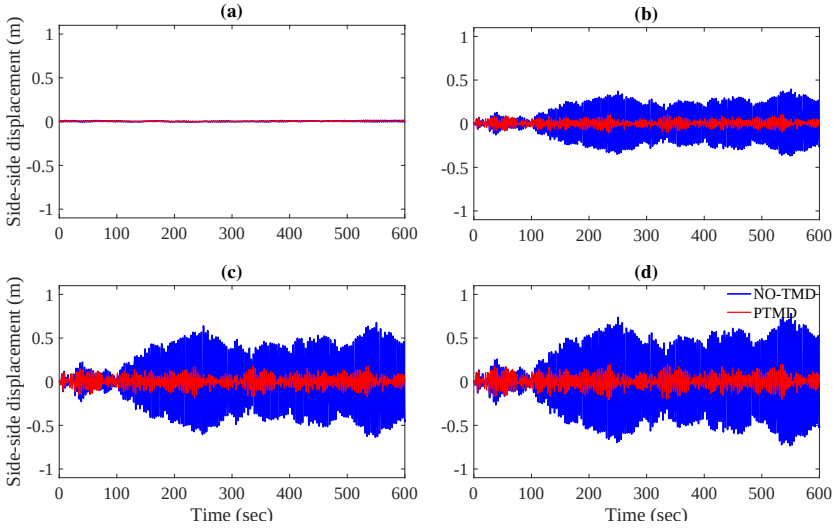

Figure 11: Nacelle side-side vibration comparison with and without the 3d-PTMD under four different wind-wave misalignment angles. (a): $\beta = 0°$ (b): $\beta = 30°$, (c): $\beta = 60°$, (d): $\beta = 90°$.

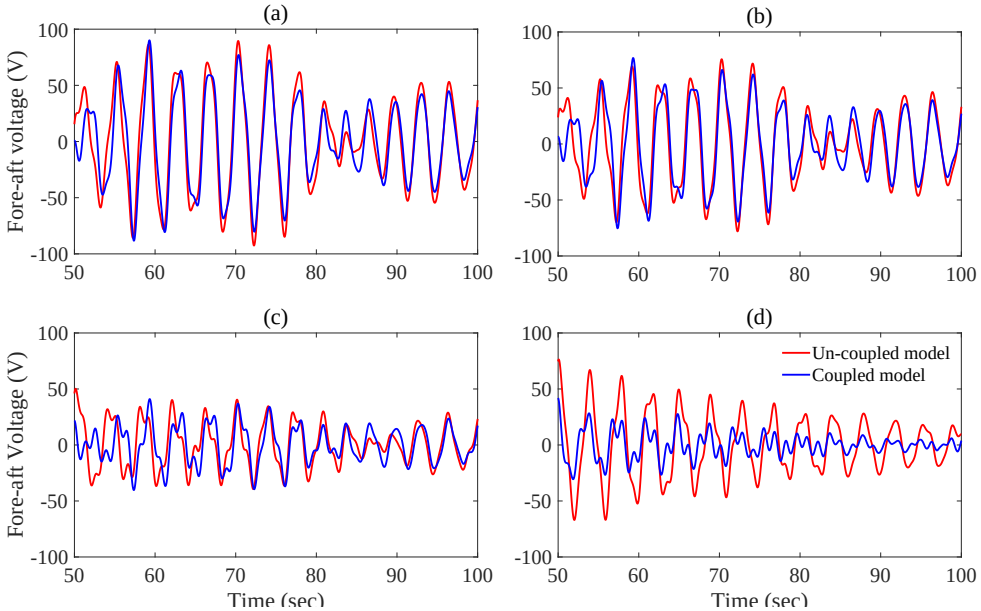

Figure 12: Comparison of generated electrical voltage between coupled and uncoupled models in fore-aft direction under different wind-wave misalignment angles. (a): $\beta = 0°$ (b): $\beta = 30°$, (c): $\beta = 60°$, (d): $\beta = 90°$.

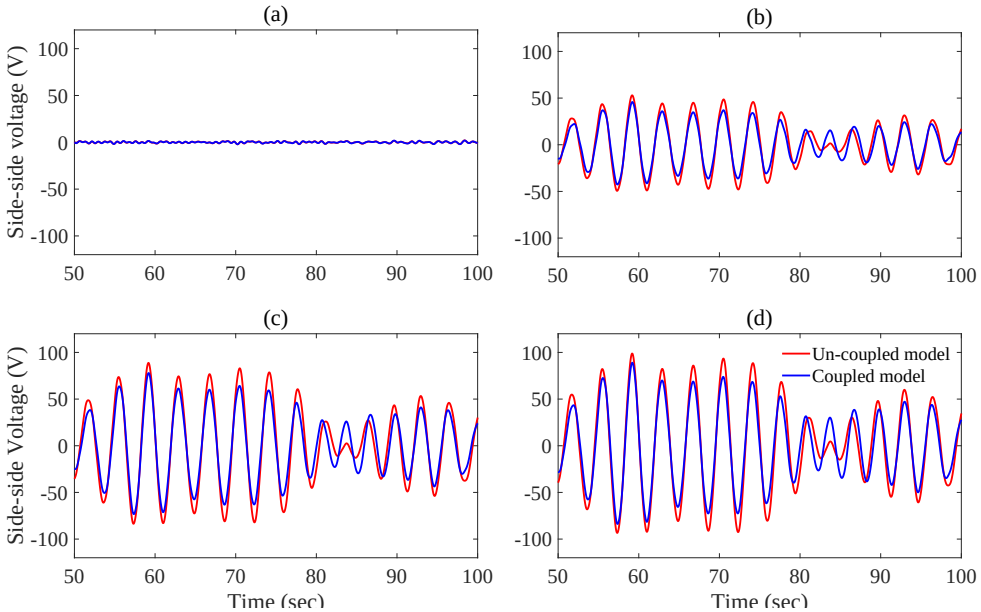

Figure 13: Comparison of generated electrical voltage between coupled and uncoupled models in side-side direction under different wind-wave misalignment angles. (a): $\beta = 0°$ (b): $\beta = 30°$, (c): $\beta = 60°$, (d): $\beta = 90°$.

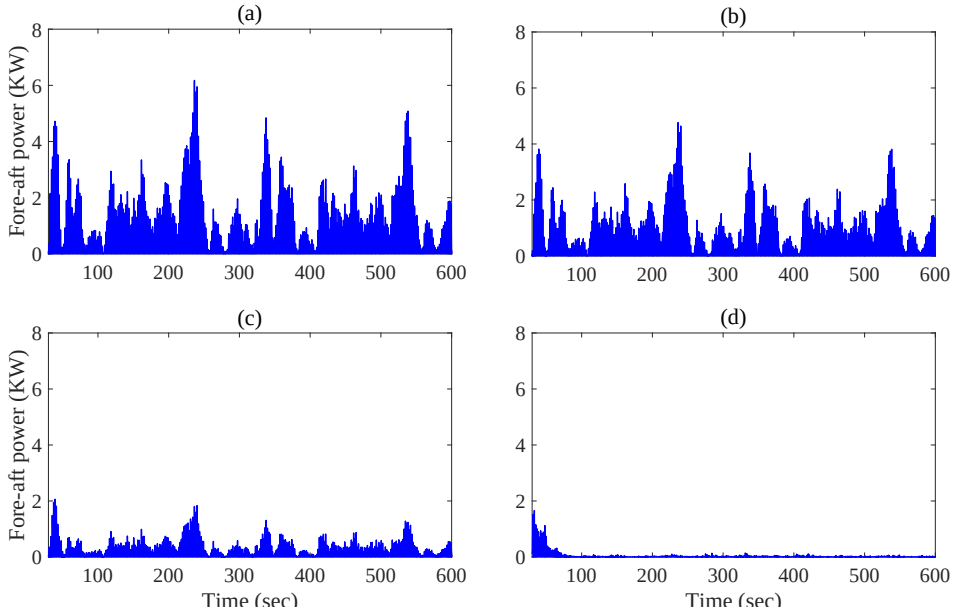

Figure 14: Generated electrical power in fore-aft direction under different wind-wave misalignment angles. (a): $\beta = 0°$ (b): $\beta = 30°$, (c): $\beta = 60°$, (d): $\beta = 90°$.

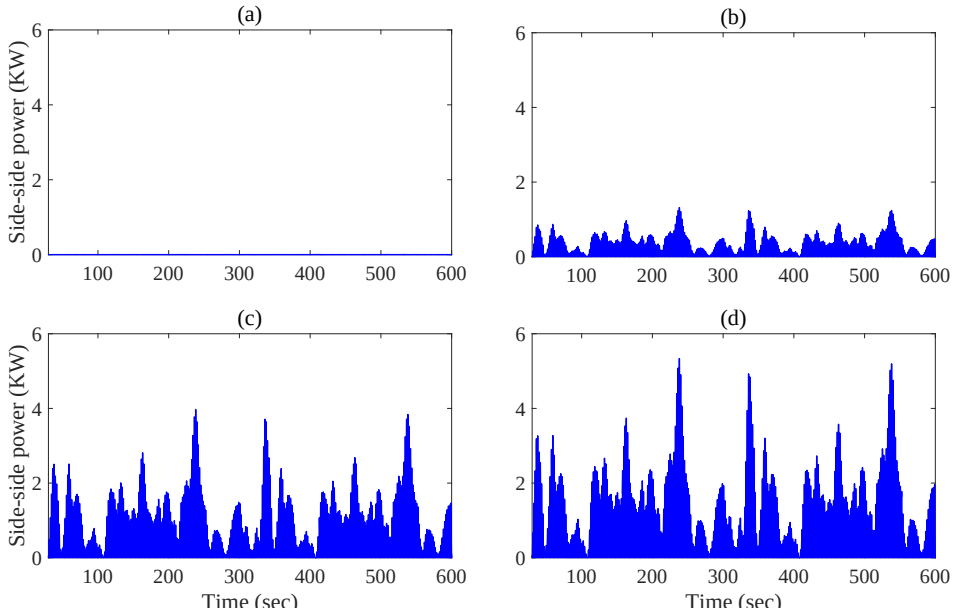

Figure 15: Generated electrical power in side-side direction under different wind-wave misalignment angles. (a): $\beta = 0°$ (b): $\beta = 30°$, (c): $\beta = 60°$, (d): $\beta = 90°$.

7. Conclusions

In the present paper, a 3d-PTMD with an energy harvester is utilized to control the bi-directional vibration of the monopile OWTs through converting the kinetic energy into electrical power. An analytical model of the monopile OWT coupled with the 3d-PTMD and the energy harvester is established. Linear electromagnetic devices are used instead of traditional viscous dampers to convert the kinetic energy of the pendulum into electrical power. The performance of the 3d-PTMD energy harvester system in reducing the response and harvesting the kinetic energy is evaluated. Based on the presented results, the following conclusions can be obtained:

1. The 3d-PTMD energy harvester system is able to reduce the nacelle vibrations in the fore-aft and side-side directions significantly. Quantitatively, the 3d-PTMD can reduce the nacelle RMS response by 70% in the fore-aft direction and 77% in the side-side direction.

2. Instead of dissipating the kinetic energy into heat, the linear electromagnetic devices are implemented to convert the motion of the 3d-PTMD into electrical power. Theoretical results indicate that considerable amount of energy (with a magnitude of KW) can be produced which can be used to power sensors and actuators for the structural health monitoring and control systems.

3. The difference of the generated electrical voltage between coupled and uncoupled energy harvester models is around 7% using the parameter values selected in the present study. The small difference for the generated electrical power between the coupled and uncoupled energy harvester is because of the low frequency feature of the primary system and small value of coil inductance. It can be concluded that for low frequency structures such as high-rise buildings, bridges, OWTs and etc. uncoupled equations for the energy harvester can be used with a good accuracy.

4. Theoretically, the generated electrical power using electromagnetic energy harvester is in orders of magnitude of kilowatts which is a considerable amount of energy to power the structural health monitoring and control devices. It is important to consider the practical constraints and determine the applicable generated electrical power. Therefore, experimental analysis to evaluate the findings of this paper will be implemented in future study.

Acknowledgment

This work was supported by Louisiana State University Start-up Fund (fund number is 127150013), the Faculty Research Grant (fund number is 127159132) and the Innovation in Engineering Research (FIRE) Grant provided by the College of Engineering at Louisiana State University. This work was also supported by Key Laboratory of Performance Evolution and Control for Engineering Structures of Ministry of Education, Tongji University (Grant No. 2018KF-6). The authors are grateful for all the support.

References

[1] P. Murtagh, A. Ghosh, B. Basu, B. Broderick, Passive control of wind turbine vibrations including blade/tower interaction and rotationally sampled turbulence, Wind Energy. 11 (2007) 305–317.

[2] S. Colwell, B. Basu, Tuned liquid column dampers in offshore wind turbines for structural control, Engineering Structures. 31 (2009) 358–368.

[3] M. Lackner, M. Rotea, Structural control of floating wind turbines, Mechatronics. 21 (2011) 704-719.

[4] A. Staino, B. Basu, S. Nielsen, Actuator control of edgewise vibrations in wind turbine blades, J. Sound Vib. 331 (2012) 1233–1256.

[5] B. Fitzgerald, B. Basu, Cable connected active tuned mass dampers for control of in-plane, J. Sound Vib. 333 (2014) 5980–6004.

[6] C. Sun, Semi-active control of monopile offshore wind turbines under multi-hazards. Mechanical Systems and Signal Processing. 99(15) (2018) 285-305.

[7] C. Sun, Mitigation of offshore wind turbine responses under wind and wave loading: Considering soil effects and damage. Structural Control Health Monitoring. 25 (2018).

[8] V. N. Dinh, B. Basu, S. Nagarajaiah, Semi - Active Control of Vibrations of Spar Type Floating Offshore Wind Turbines. Smart Structures and Systems. 18 (2016) 683-705.

[9] M. Lackner, M. Rotea, Passive structural control of offshore wind turbines, Wind Energy. 14 (2011) 373-388.

[10] C. Sun, V. Jahangiri, Bi-directional vibration control of offshore wind turbines using a 3D pendulum tuned mass damper, Mechanical System and Signal Processing. 105 (2018) 338-360.

[11] C. Sun, V. Jahangiri, Fatigue damage mitigation of offshore wind turbines under real wind and wave conditions, Engineering Structures. 178 (2019) 472-483.

[12] G. Housner et al., Structural control: past, present, and future, Journal of Engineering Mechanics. 123(9) (1997) 897-971.

[13] D. Xie et al., Energy harvesting from high-rise buildings by a piezoelectric coupled cantilever with a proof mass, International Journal of Engineering Science. 72 (2013) 98-106.

[14] A. Shen, S. Zhu, L. Xu, An experimental study on self-powered vibration control and monitoring system using electromagnetic TMD and wireless sensors, Sensors and Actuators: A: Physical. 180 (2012) 166-176.

[15] X. Tang, L. Zuo, Simultaneous energy harvesting and vibration control of structures with tuned mass dampers, Journal of Intelligent Material Systems and Structures. 23 (2012) 2117-2127.

[16] R. Arias, J. Connor, J. Ochsendorf, Feasibility study of passive electromagnetic damping systems, Journal of Structural Engineering. 134 (2008) 164-170.

[17] V. Jahangiri, H. Mirab, R. Fathi, M.M. Ettefagh, TLP structural health monitoring based on vibration signal of energy harvesting system, American Journal of Solids and Structures. 13 (2016) 897-915.

[18] M. J. Muliawan, M. Karimirad, T. Moan, Dynamic response and power performance of a combined spar-type floating wind turbine and coaxial floating wave energy converter, Renewable Energy. 50 (2013) 47-57

[19] C. Sun, S. Nagarajaiah, A. J. Dick, Experimental Investigation of Vibration Attenuation Using Nonlinear Tuned Mass Damper and Pendulum Tuned Mass Damper in Parallel, Nonlinear Dynamics. 78(4) (2014) 2699-2715.

[20] C. Sun, S. Nagarajaiah, A. J. Dick, Family of Smart Tuned Mass Dampers with Variable Frequency under Harmonic Excitations and Ground Motions: Closed-Form Evaluation, Smart Structures and Systems. 13(2) (2014) 319-341.

[21] B.J. Jonkman, L. Kilcher, TurbSim User's Guide: Version 1.06.00 *National Renewable Energy Laboratory* 2012; Technical Report.

[22] Hansen MOL. Aerodynamics of wind turbines. *James & James (Science Publishers) Ltd* 2000.

[23] Faltinsen OM. *Sea Loads on Ships and Offshore Structures.* Cambridge University Press: Cambridge, UK, 1990.

[24] IEC. *Wind turbines. Part 3: design requirements for offshore wind turbines.* IEC 61400-3 (ed. 1) 2009, Geneva, Switzerland: International Electrotechnical Commission.

[25] Jonkman J., Butterfield S., Musial W., Scott G. *Definition of a 5-MW Reference Wind Turbine for Offshore Systems Development.* Technical Report,NREL 2009.

[26] Carswell W., Johansson J., Lovholt F., Arwade S.R., Madshus C., DeGroot D.J., Myers A.T., Foundation damping and the dynamics of offshore wind turbine monopiles. Renewable Energy 80 (2015) 724–736.